misprint in Eq. (V.26). Two hole-creation operators $b^+(p_1)b^+(p_2)$ should be inserted at the end of the first line.

[17]See Ref. 14, Eq. (V.27).

[18]N. M. Hugenholtz, Physica 23, 481 (1957).

[19]E. J. Irwin, Ph.D. thesis, Cornell University, 1963 (unpublished), available from University Microfilms, Inc., order No. 64-1010; C. M. Ko and D. W. Sprung, Can. J. Phys. 47, 123 (1969).

[20]E. P. Harper, Y. E. Kim, and A. Tubis, Phys. Rev. C 2, 877 (1970).

[21]R. Balian and E. Brézin, Nuovo Cimento 61B, 403 (1969).

[22]B. H. Brandow, Phys. Rev. 152, 863 (1966).

[23]A. Kallio and B. D. Day, Nucl. Phys. A124, 177 (1969).

PHYSICAL REVIEW C VOLUME 6, NUMBER 6 DECEMBER 1972

# Elastic *pd* Scattering at 316, 364, 470, and 590 MeV in the Backward Hemisphere

J. C. Alder,*†‡ W. Dollhoff,‡ C. Lunke,†‡ C. F. Perdrisat,‡ W. K. Roberts, P. Kitching,§¶ G. Moss,§¶ W. C. Olsen,§¶ and J. R. Priest‖

*National Aeronautics and Space Administration, Lewis Research Center, Cleveland, Ohio 44135*

(Received 5 July 1972)

The results of an investigation of the elastic *pd* differential cross section for center-of-mass angles between 91 and 164° at energies of 316, 364, 470, and 590 MeV are presented. For center-of-mass scattering angles larger than 130°, the cross sections at any given angle are within 10% of each other for the three largest energies. The extrapolated 180° differential cross section observed in this experiment remains nearly constant from 316 to 590 MeV. This is in marked contrast to the rapid decrease in cross section with increasing energy observed by other investigators for both larger and smaller energies. Possible theoretical explanations of this behavior are mentioned.

## INTRODUCTION

It has been known for some time that above 300 MeV, the backward elastic (*pd*) differential cross section was larger than one would expect on the basis of a single-nucleon-exchange mechanism. There was a renewed interest in this problem when data at 1300[1] and 1000 MeV,[2] and later 590 MeV[3] became available. A possible explanation of the anomalous backward scattering was proposed by Kerman and Kisslinger[4] in terms of an admixture of excited nucleon states in the ground state of the deuteron. It was found that if the probability for the ground state of the deuteron to be a normal nucleon and a $(\frac{5}{2}, \frac{1}{2})$ nucleon isobar with invariant mass 1688 MeV, was 2%, the results of experiments of Refs. 2 and 3 could be explained. The 1688-MeV isobar is the lowest nucleon excited state that can exist in the deuteron, unless both nucleons are excited. The different possible components of the deuteron ground state with isobars are discussed for example by Arenhövel, Danos, and Williams.[5]

Another model was proposed by Craigie and Wilkin[6] who argued that for laboratory energies around 600 MeV, triangular graphs with a neutron line and a pion line connecting the observed states should be more important than the one-neutron-exchange diagram. A neutron-pion-exchange graph is probably dominant in the process $pp \to d\pi^+$, which is known to have a resonant-like behavior with a maximum at 600 MeV. The resonant behavior in $d\pi^+$ final state is believed to be associated with the $(\frac{3}{2}, \frac{3}{2})$ 1236-MeV resonance in the nucleon-pion system, which would enhance reactions in which the nucleon and pion exchanged have an invariant mass near that of the $(\frac{3}{2}, \frac{3}{2})$ resonance. This situation occurs also in the *pd* system, Wilkin[7] calculated the (*pd*) elastic cross section near 180° with no free parameter and obtained excellent agreement with the data of Ref. 3.

In still another effort to understand (*pd*) scattering, Remler and Miller[8] have been investigating the lower-energy data in terms of single-nucleon exchange, single-scattering and multiple-scattering contributions. The data below 300 MeV are being used to determine a number of parameters to describe the third contribution. An extrapolation of these parameters to the energy region where other mechanisms may be important is expected to demonstrate the existence of new terms in the interaction.

At the inception of this experiment very little data outside of that previously mentioned existed above 300 MeV. Experimental data had been reported at 340[9] and 660 MeV[10] but included only a few data points in the backward hemisphere, each with relatively large uncertainties. The current

strong interest in the *pd* system therefore seemed to justify a systematic investigation of the large-angle region for the elastic channel as a function of energy. About the time this experiment was performed Booth *et al.*[11] reported data obtained at 415 MeV. The 415-MeV data are in excellent qualitative and quantitative agreement with the data reported here.

The 590-MeV results obtained in this experiment are systematically lower than those obtained in a counter experiment and published in Ref. 3. After reviewing the earlier data we attribute this discrepancy to the incomplete subtraction of inelastic events in that analysis.

## DESCRIPTION OF THE EXPERIMENTAL SETUP

Figure 1 is a drawing of the experimental arrangement. The experiment was performed at 4 energies 590, 470, 364, and 316 MeV at the National Aeronautics and Space Administration Space Radiation Effects Laboratory. Beams with energies lower than the normal 590-MeV beam were obtained by placing copper degraders in the upstream part of the transport system. The beam spot at the target position at 590 MeV was 1.8 by 2.5 cm (horizontal by vertical). The beam divergence was less than ±1°. It was not possible to maintain this size with degraded beam energies

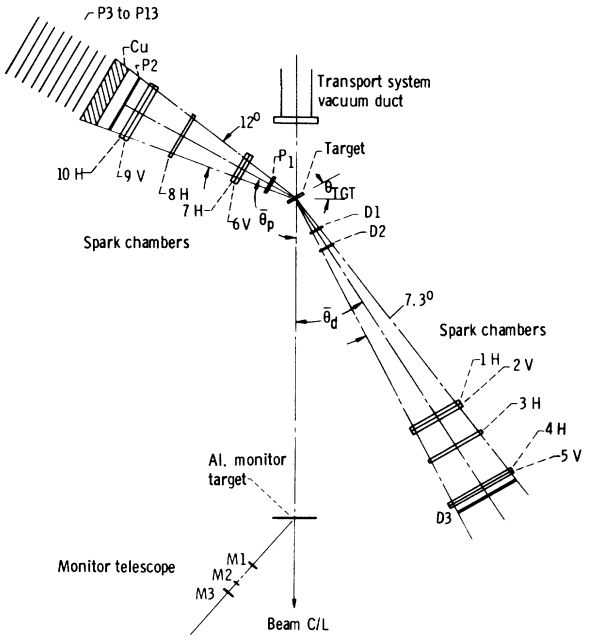


FIG. 1. Experimental setup. $D_1$, $D_2$, $D_3$, and $P_1$, $P_2$ are scintillation counters defining an event. 1H, 2V··· 10H are wire-spark-chamber planes (H for horizontal, V for vertical coordinate). $P_3$ to $P_{13}$ are elements of the range telescope.

without adversely affecting the beam divergence. As a consequence, the beam spots on target at the reduced energies were 3.7 by 5.0 cm, 3.7 by 3.7 cm, and 4.0 by 4.0 cm at 470, 364, and 316 MeV, respectively. Divergence was maintained at less than ±1.5°.

The incident proton intensity was monitored by scattering protons into a 3-counter telescope from an auxiliary aluminum target 0.6 cm thick placed 6 m downstream from the $CD_2$ target. The monitor target was 30 by 30 $cm^2$ and pictures were taken for each beam energy to insure that the beam size at the monitor target did not exceed the monitor telescope's 100% acceptance cone. The beam monitor was calibrated using the $^{12}C(p, pn)^{11}C$ reaction[12] on graphite targets. A monitor calibration was made for each new beam energy but was not repeated every time the same energy was set up, except for the 364-MeV beam. The two calibrations at this energy gave results different by 2 standard deviations (the standard deviation for each calibration is about 1.5%; the absolute uncertainty due to the probable error of the $^{12}C(p, pn)^{11}C$ cross section is 5% for each energy).

A single $CD_2$ target (hydrogen content less than 2%) 0.203 cm thick by 10 cm by 10 cm was used throughout the experiment. It was oriented so as to minimize multiple scattering of the backward-scattered proton. Graphite targets 0.063 and 0.381 cm thick were used to measure the background contribution from the carbon in $CD_2$. The thin graphite target had 66% of the number of C nuclei in the $CD_2$ target, and the thick one 4 times as many as in the $CD_2$ target.

The detection apparatus was a coincidence spectrometer (see Fig. 1). Deuterons scattered in the forward center-of-mass hemisphere were detected by three scintillators $D_1$, $D_2$, $D_3$, and three spark chambers. The three spark chambers provided three horizontal and two vertical coordinates. Counter $D_1$ was 45.8 cm from the target, 0.21 cm thick, and 7.6 cm high by 10.8 cm wide. Counter $D_2$ was 61 cm from the target, 0.21 cm thick, and 7.9 cm high by 11.1 cm wide. Counter $D_3$ was 600 cm from the target, 0.63 cm thick, and 25.4 cm high by 76.2 cm wide. The three spark chambers were located at 438.7, 498.7, and 589.3 cm from the target, and had sensitive regions larger than the solid angle defined by $D_1$, $D_2$, and $D_3$. Protons with laboratory angles larger than 95° were detected in two scintillators $P_1$, $P_2$ and a set of three spark chambers. These spark chambers also provided three horizontal and two vertical coordinates. Detector $P_1$ was 51 cm from the target, 0.203 cm thick, and 12.7 cm wide by 5.7 cm high. Detector $P_2$ was 0.63 cm thick and 28 cm wide by 12.7 cm high. Detector $P_2$ was from

122 to 161 cm from the target during the experiment depending on the proton angle. The spark chambers had sensitive regions larger than the solid angle defined by $P_1$ and $P_2$. For proton laboratory angles smaller than 95°, a range telescope was added to the proton detector. The range counters greatly decreased the background originating mostly from $(p, 2p)$ reaction on D and C. This background contribution became more and more important as the sum angle $(\theta_p + \theta_d) \approx 82°$, characteristic of $pp$ scattering, was approached. The range counter consisted of a copper energy degrader placed directly behind $P_2$ ($P_2$ was reduced in size to 7.6 cm high by 6.35 cm wide) and a close-packed array of 11 scintillation counters $P_3$ to $P_{13}$ immediately behind the energy degrader (counters $P_3$ to $P_{13}$ were 17.8 cm high by 12.7 cm wide by 0.63 cm thick). The energy degrader was selected so that protons of interest would stop somewhere in the stack of counts $P_3$ to $P_{13}$. Typically, the Bragg peak was 2 to 3 counters wide. The spark planes were of the copper-nylon-mesh type (copper wire 0.0125 cm diam, spacing 0.05 cm) with magnetostriction readout.

A coincident event was defined as EVENT = $(D_1 \times D_2 \times D_3) \times (P_1 \times P_2)$, or $(D_1 \times D_2 \times D_3) \times (P_1 \times P_2 \times P_3)$ when the range telescope was used. The master logic timing signal in EVENT was obtained from detector $D_2$. The time of flight of the particle detected in the deuteron arm was measured for each EVENT using EVENT as a start signal and the logic signal from detector $D_3$ as the stop signal for a time-to-amplitude converter. The time-to-amplitude signal was digitized in a 1024-channel analog-to-digital converter. When the range counter was used the outputs from the range counters $P_4$ to $P_{13}$ were fed to a gated latching coincidence circuit, latched by EVENT. EVENT was also used to trigger a 5-kV pulse generator which drove a master spark gap. The master spark gap then triggered a number of spark gaps which provided the high-voltage pulses for the various spark chambers. Spark-position information was processed in a commercial digitizing system.

The digitized time-of-flight signal and spark-position information and the range information were interfaced with the Space Radiation Effects Laboratory on-line computer and read into the computer and onto magnetic tape EVENT by EVENT. A direct on-line attempt at geometric reconstruct was performed EVENT by EVENT (this allowed a check of the progress of the experiment). In the on-line mode the basic critereon for a good event was that the reconstructed trajectories in the two arms of the spectrometer intersect the target plane within a prescribed distance around the beam line. To insure the maximum number of reconstructions in the on-line mode the "cuts" on the target intercept were made larger than the physical target. This was done to insure that any loss due to multiple scattering would be negligible.

On the basis of the known spatial resolution of the spark chambers and the reaction kinematics it was expected that a sufficient criterion to reject inelastic events for proton angles greater than 95° in the laboratory would be the angular correlation of the proton and deuteron. For proton laboratory angles smaller than 95° selection of the deuteron by time of flight and proton energy by range were considered necessary to reduce the inelastic contributions to manageable levels. The analysis of the data confirmed these initial assumptions. During final off-line replay analysis appropriate "cuts" were applied to the range and time-of-flight information along with a tightening of the "cuts" applied to the target intercept.

Most of the data presented in this work were taken in the range of laboratory proton angles between 95 and 145°. These were obtained with the deuteron-detector center angles of 20, 12.5, and 10° in the laboratory. The horizontal proton detector aperture was 10, 12, and 13°, respectively, for the three deuteron angles above. The horizontal aperture of the deuteron counters was maintained constant at 7.3°. The aperture information given here refers to a point target. In the c.m. system for the $pd$ final states, the forward horizontal acceptance was very nearly twice the backward acceptance. Therefore for every position of the forward leg the proton telescope was placed in two different positions in order to cover completely the forward acceptance. The experiment was planned with horizontal acceptances closely matched in the c.m. in order to minimize the number of spectrometer arm-position changes. In the vertical direction however, the angular acceptance was generally determined by counter $P_2$. For proton angles smaller than 95°, the defining counter in the proton arm defined a constant solid angle with 3° horizontal aperture. At the smallest proton angle studied, 60° in the laboratory, the vertical acceptance was limited in the forward arm of the spectrometer. Cuts applied in the vertical plane of the proton arm during replay analysis insured 100% transmission for events defined by the reduced proton solid angle of acceptance.

## ANALYSIS OF THE DATA

As soon as the information associated with each event was placed in buffer regions of the computer memory, an attempt at geometrical reconstruction

was made directly on line, (allowing a check of the progress of the experiment). The data discussed here are the result of a later replay of the data tapes using essentially the same routines as during the run, although with different cuts on some of the parameters.

Eight of the ten spark-plane coordinates were associated with four digitizer scalers each, the remaining two coordinates with two scalers. Although the spark multiplicity in any of the coordinates was always small (at the most 30% double sparks, 1 to 3% triples), the reconstruction routines were such that several spark combinations could be tried for a given event, until one satisfying all criteria was found. The fraction of events that required more than one attempt remained small (of the order of a few percent), in part because all of the cuts applied were wide. The effect of increasingly narrow cuts was studied off line. For each acceptable event the following quantities were calculated and stored for display at the end of a run (a typical run contained 10 000 events): (1) time of flight; (2) distribution of the distance to the spark in the middle horizontal plane for the selected trajectory in the deuteron and proton detectors (a check of the plane spacial resolution); (3) intersections of both trajectories with the target in horizontal and vertical directions, and the distance between intersections of the two trajectories in the vertical and horizontal directions (check of the correlated origin of the event); (4) scattering angles in horizontal and vertical directions $\theta_p$ and $\theta_d$, $x_p$ and $x_d$, respectively; (5) coplanarity of the two trajectories calculated as the difference of the vertical angles projected in a plane perpendicular to the beam at the target; (6) EVENTS as a function of $\theta_p + \theta_d$ sorted into bins $\Delta\theta_p$ wide; and (7) range.

To avoid the need of maintaining one of the c.m. solid angles larger than the other to minimize border and resolution effects, we classified the events in bins on the proton scattering angle $\theta_p$ and displayed for each of these bins the complete correlation spectrum in the sum angles $(\theta_p + \theta_d)$. Each proton-angle bin could then in first order be considered as a subexperiment with complementary-angle condition on the deuteron side satisfied, allowing for kinematics, multiple scattering of the particles in the different counters and target, and intrinsic spatial resolution of the spark planes. The background from the graphite target was measured for every angle and for every energy. The subtraction of the C contribution was made taking into account the numbers of carbon nuclei in the $CD_2$ and graphite targets and the number of incident protons in the $CD_2$ and graphite runs. Checks of the C substraction were made both on the time-of-flight and angular-correlation spectra. When no time-of-flight cuts were applied, the continum under the elastic peak in the correlation spectra was always more important; but we obtained the same cross sections within statistical error, whether we applied cuts on the time of flight or not. We also verified that when the C subtraction did not remove the background in the correlation spectra completely, an artificial increase of the C spectrum compatible with the time-of-flight spectra would not affect the results by more than 1 standard deviation.

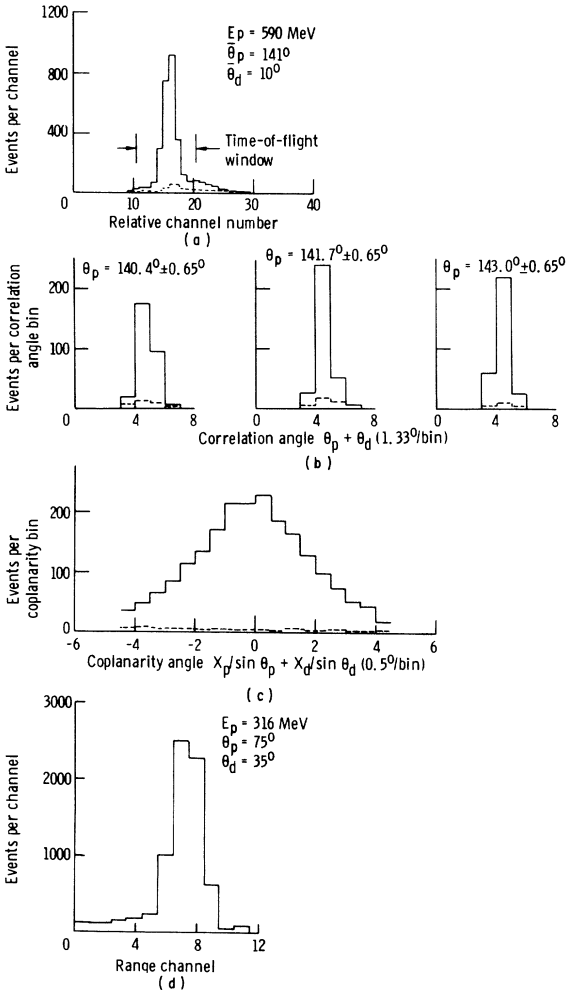


FIG. 2. Typical spectra obtained in this experiment. (a) gives a time-of-flight spectrum, (b) the distribution $(\theta_p + \theta_d)$ for three different values of $\theta_p$, the proton scattering angle, and (c) shows the coplanarity angle spectrum defined as $(x_p/\sin\theta_p) + (x_d/\sin\theta_d)$. (d) is a range spectrum obtained in a different geometry and at an energy different from those of (a), (b), and (c), namely $\theta_p = 75°$ and $E_p = 316$ MeV.

## CALCULATIONS OF THE CROSS SECTION

The cross section for each proton bin of width $\Delta\theta_p$ around $\theta_p$ was calculated from

$$\frac{d\sigma}{d\Omega_p}=\frac{N(\theta_p)\times\cos\theta_{\rm tgt}}{\Delta\Omega_p\times n\times I\times\epsilon_{\rm sc}};\quad \Delta\Omega_p=\frac{\Delta\theta_p}{57.3}\times\frac{\text{height of } P_2}{\text{distance to } P_2},$$

where $N(\theta_p)=[(N_{CD_2}(\theta_p)-N_c(\theta_p)]$ is the number of elastic scattering events (after proper background subtraction) having good trajectories and where applicable good time of flight and range, $\theta_{\rm tgt}$ is the angle of the target plane with the normal to the beam, $n$ is the number of deuterium nuclei within the $CD_2$ target. $I$ = (Monitor)×(Calibration) is the number of incident protons in a run. $\epsilon_{\rm sc}$ is the over-all spark-plane efficiency, and includes both sparking and reconstruction efficiencies. We evaluated $\epsilon_{\rm sc}$ as the ratio of the total number of reconstructed events in a run that satisfy a number of conditions described below (and which did not include time of flight), to the number of "true" triggers (EVENT), defined as the difference between real triggers and chance coincidences $\overline{\rm EVENT}=(D_1\times D_2\times D_3)$ 56 nsec delay $(P_1\times P_2)$. Implied in the definition of "true" triggers is the assumption that chance coincidence $\overline{\rm EVENT}$ were not reconstructed; we verified experimentally that $\overline{\rm EVENT}$ triggers had less than 5% probability to be reconstructed. $\epsilon_{\rm sc}$ was found to vary from experimental run to experimental run, (this variation was correlated with the beam duty factor.) It was found that the cross sections calculated for each run for a given geometry and energy were equal within statistics indicating a negligible systematic error in the definition of $\epsilon_{\rm sc}$. To determine if $\epsilon_{\rm sc}$ introduced an absolute error in the cross-section calculations, the 590-MeV, 90° c.m., $p$-$p$ differential cross section was measured. The value obtained was $2.74\pm0.16$ mb/sr which agrees with the value of $2.58\pm0.05$ mb/sr reported in Ref. 3. Despite these checks we have ascribed a possible ±4% error to the values of $\epsilon_{\rm sc}$ used in the cross-section calculations.

The condition imposed on reconstruction were of three types. First, each group of horizontal and vertical planes on the deuteron and proton

TABLE I. $p\,d$ differential cross section at 590 MeV.

| Proton laboratory scattering angle $\theta_{p\,\rm lab}$ (deg) | Laboratory differential cross section and error $\left(\frac{d\sigma}{d\Omega}\right)_{\rm lab}\pm\Delta\left(\frac{d\sigma}{d\Omega}\right)_{\rm lab}$ (μb/sr) | Proton center-of-mass scattering angle $\theta_{p\,\rm c.m.}$ (deg) | $\cos\theta_{p_{\rm c.m.}}$ | Center-of-mass differential cross section and error $\left(\frac{d\sigma}{d\Omega}\right)_{\rm c.m.}\pm\Delta\left(\frac{d\sigma}{d\Omega}\right)_{\rm c.m.}$ (μb/sr) | Momentum transfer squared $-t$ $(\rm GeV/c)^2$ |
|---|---|---|---|---|---|
| 60 | 44.7±1.2 | 92.7 | −0.047 | 30.4±0.8 | 1.06 |
| 71 | 25.9±0.5 | 106.1 | −0.277 | 22.1±0.45 | 1.28 |
| 77.75 | 18.0±0.4 | 113 | −0.39 | 17.6±0.4 | 1.40 |
| 85.5 | 14.6±0.3 | 121.6 | −0.524 | 17.4±0.35 | 1.54 |
| 95.5 | 16.2±1.4 | 130.9 | −0.655 | 24.6±2.2 | 1.67 |
| 97.5 | 16.9±1.4 | 132.6 | −0.677 | 26.7±2.2 | 1.70 |
| 99.5 | 18.9±1.4 | 134.3 | −0.698 | 31.3±2.3 | 1.72 |
| 101.5 | 20.0±1.4 | 136.0 | −0.719 | 34.9±2.5 | 1.74 |
| 105.5 | 23.3±1.3 | 139.1 | −0.756 | 44.3±2.5 | 1.78 |
| 107.5 | 24.4±1.3 | 140.7 | −0.774 | 48.5±2.6 | 1.79 |
| 109.5 | 24.4±1.2 | 142.2 | −0.790 | 50.0±2.5 | 1.81 |
| 111.5 | 28.5±1.3 | 143.6 | −0.805 | 62.1±2.8 | 1.83 |
| 118.4 | 31.8±1.0 | 148.4 | −0.852 | 81.3±2.6 | 1.87 |
| 120.8 | 33.6±1.0 | 150.0 | −0.866 | 90.1±2.7 | 1.89 |
| 123.2 | 37.0±1.0 | 151.5 | −0.877 | 104.0±3.0 | 1.90 |
| 125.6 | 36.9±1.0 | 153.0 | −0.891 | 108.0±2.9 | 1.91 |
| 130.5 | 39.4±1.6 | 155.9 | −0.913 | 125.0±5.0 | 1.93 |
| 132.5 | 37.6±1.6 | 157.1 | −0.921 | 124.0±5.0 | 1.94 |
| 134.6 | 39.8±1.6 | 158.2 | −0.929 | 136.0±6.0 | 1.95 |
| 136.6 | 39.7±1.6 | 159.3 | −0.935 | 141.0±6.0 | 1.95 |
| 137.2 | 39.6±1.5 | 159.7 | −0.938 | 140.0±5.0 | 1.96 |
| 139.8 | 41.8±1.5 | 161.1 | −0.946 | 155.0±6.0 | 1.97 |
| 142.4 | 44.0±1.5 | 162.4 | −0.953 | 170.0±6.0 | 1.97 |
| 145.0 | 45.2±1.5 | 163.8 | −0.960 | 182.0±6.0 | 1.98 |

TABLE II. $pd$ differential cross section at 470 MeV.

| Proton laboratory scattering angle $\theta_{p\,\mathrm{lab}}$ (deg) | Laboratory differential cross section and error $\left(\frac{d\sigma}{d\Omega}\right)_{\mathrm{lab}} \pm \Delta\left(\frac{d\sigma}{d\Omega}\right)_{\mathrm{lab}}$ ($\mu$b/sr) | Proton center-of-mass scattering angle $\theta_{p\,\mathrm{c.m.}}$ (deg) | $\cos\theta_{p\,\mathrm{c.m.}}$ | Center-of-mass differential cross section and error $\left(\frac{d\sigma}{d\Omega}\right)_{\mathrm{c.m.}} \pm \Delta\left(\frac{d\sigma}{d\Omega}\right)_{\mathrm{c.m.}}$ ($\mu$b/sr) | Momentum transfer squared $-t$ (GeV/$c$)$^2$ |
|---|---|---|---|---|---|
| 60 | 64.2 ± 1.4 | 91.4 | −0.025 | 43.5 ± 0.95 | 0.82 |
| 71 | 39.0 ± 0.7 | 104.9 | −0.257 | 33.0 ± 0.6 | 1.01 |
| 78.25 | 29.7 ± 0.75 | 113.0 | −0.39 | 29.4 ± 0.75 | 1.12 |
| 86 | 22.3 ± 0.55 | 121.0 | −0.515 | 26.1 ± 0.65 | 1.22 |
| 97.5 | 21.6 ± 0.9 | 131.7 | −0.665 | 32.5 ± 1.3 | 1.33 |
| 99.5 | 23.5 ± 0.9 | 133.4 | −0.687 | 37.2 ± 1.4 | 1.35 |
| 102 | 23.4 ± 0.7 | 135.5 | −0.713 | 39.2 ± 0.8 | 1.37 |
| 105.5 | 28.4 ± 0.9 | 138.3 | −0.747 | 51.8 ± 1.5 | 1.40 |
| 107.5 | 28.5 ± 0.9 | 139.9 | −0.765 | 54.4 ± 1.6 | 1.42 |
| 109.5 | 31.6 ± 0.9 | 141.4 | −0.781 | 62.1 ± 1.7 | 1.43 |
| 112 | 33.6 ± 0.7 | 143.2 | −0.801 | 70.7 ± 1.5 | 1.44 |
| 118.4 | 39.7 ± 1.1 | 147.7 | −0.845 | 95.9 ± 2.6 | 1.48 |
| 120.8 | 42.1 ± 1.1 | 149.4 | −0.861 | 107.0 ± 3.0 | 1.49 |
| 123.2 | 44.5 ± 1.1 | 150.9 | −0.874 | 119.0 ± 3.0 | 1.50 |
| 125.6 | 44.6 ± 1.1 | 152.4 | −0.886 | 124.0 ± 3.0 | 1.51 |
| 129.9 | 46.1 ± 1.3 | 155.0 | −0.906 | 135.0 ± 4.0 | 1.53 |
| 132.3 | 47.1 ± 1.3 | 156.4 | −0.916 | 146.0 ± 4.0 | 1.54 |
| 134.7 | 50.6 ± 1.3 | 157.8 | −0.926 | 163.0 ± 4.0 | 1.54 |
| 137.1 | 51.4 ± 1.3 | 159.2 | −0.935 | 172.0 ± 4.0 | 1.55 |
| 139.7 | 44.5 ± 1.0 | 160.6 | −0.943 | 156.0 ± 4.0 | 1.56 |
| 142.3 | 45.8 ± 1.0 | 162.0 | −0.951 | 167.0 ± 4.0 | 1.56 |
| 144.9 | 45.6 ± 1.0 | 163.4 | −0.958 | 173.0 ± 4.0 | 1.57 |

TABLE III. $pd$ differential cross section at 364 MeV.

| Proton laboratory scattering angle $\theta_{p\,\mathrm{lab}}$ (deg) | Laboratory differential cross section and error $\left(\frac{d\sigma}{d\Omega}\right)_{\mathrm{lab}} \pm \Delta\left(\frac{d\sigma}{d\Omega}\right)_{\mathrm{lab}}$ ($\mu$b/sr) | Proton center-of-mass scattering angle $\theta_{p\,\mathrm{c.m.}}$ (deg) | $\cos\theta_{p\,\mathrm{c.m.}}$ | Center-of-mass differential cross section and error $\left(\frac{d\sigma}{d\Omega}\right)_{\mathrm{c.m.}} \pm \Delta\left(\frac{d\sigma}{d\Omega}\right)_{\mathrm{c.m.}}$ ($\mu$b/sr) | Momentum transfer squared $-t$ (GeV/$c$)$^2$ |
|---|---|---|---|---|---|
| 99.5 | 23.9 ± 0.6 | 132.5 | −0.676 | 37.3 ± 0.9 | 1.03 |
| 101.5 | 27.2 ± 0.7 | 134.2 | −0.697 | 43.7 ± 1.1 | 1.05 |
| 104.5 | 31.3 ± 0.8 | 136.7 | −0.728 | 55.6 ± 1.5 | 1.07 |
| 106.5 | 34.0 ± 0.9 | 138.3 | −0.747 | 63.3 ± 1.6 | 1.08 |
| 108.5 | 32.7 ± 0.9 | 139.9 | −0.765 | 63.4 ± 1.7 | 1.09 |
| 110.5 | 32.7 ± 0.9 | 141.4 | −0.782 | 66.1 ± 1.8 | 1.10 |
| 112.5 | 33.9 ± 0.9 | 142.9 | −0.798 | 71.1 ± 1.9 | 1.11 |
| 121.5 | 37.8 ± 0.9 | 149.2 | −0.859 | 95.4 ± 2.3 | 1.15 |
| 124.5 | 39.3 ± 0.8 | 151.1 | −0.876 | 105.0 ± 1.0 | 1.16 |
| 131.8 | 43.0 ± 2.1 | 155.7 | −0.911 | 131.0 ± 4.0 | 1.18 |
| 134.2 | 47.4 ± 2.2 | 157.1 | −0.921 | 150.0 ± 4.0 | 1.19 |
| 137.2 | 43.6 ± 1.9 | 158.8 | −0.932 | 144.0 ± 3.0 | 1.19 |
| 141.4 | 46.7 ± 0.9 | 161.1 | −0.946 | 164.0 ± 3.0 | 1.20 |
| 144.0 | 47.2 ± 0.9 | 162.5 | −0.954 | 172.0 ± 3.0 | 1.21 |
| 146.6 | 44.4 ± 0.9 | 163.9 | −0.961 | 168.0 ± 3.0 | 1.21 |

side (for a total of four groups) were scanned for tracks in the order HD, HP, VD, VP (for horizontal deuteron, horizontal proton, and so on). A track was defined as two sparks through which a straight line projected to the target would intercept the target within prescribed distances from the target center (either vertically or horizontally). Or, for the horizontal coordinates, where three planes were available, it was first checked whether a straight line through the first and last plane's sparks would intercept the middle plane within chosen distance from a spark in that plane; then the target-intersection test was made. Second, the events having passed the first test were checked for correlation in origin. Failure at any of the previously mentioned checks resulted in further scanning for other sparks which would give satisfactory two-correlated-track events. The fraction of true events (defined previously) that would satisfy the two tests before mentioned was usually between 70 and 80%; lower efficiencies were observed when one of the spark planes showed obvious poor sparking efficiency (usually due to insufficient gas flushing) or when the fraction of accidental coincidence in EVENT was large due to too high a beam intensity or bad stochastic properties of the beam. The fraction of accidental triggers was kept under 10% for most $CD_2$ runs, but was usually larger for graphite targets.

The third check was related to the coplanarity of the events: Two-body final states must be contained in one plane. The efficiencies calculated for coplanarity cuts of ±5° [twice the observed full width at half maximum (FWHM)] seem to be too low; the cross sections we obtain this way are systematically larger than those without coplanarity requirement. To check whether this discrepancy was related to the way the spark-chamber efficiency was evaluated, we redefined an efficiency $\epsilon'_{sc}$ as the ratio of the number of reconstructed events with a time of flight corresponding to a deuteron (±0.55 nsec/m from the elastic peak) to the number of "true" triggers within the same time-of-flight interval. It was found that $\epsilon_{sc} \sim \epsilon'_{sc}$ to within 1%. Figure 2(a) shows a typical time-of-flight spectrum for $CD_2$ and graphite targets. Figure 2(b) shows the corresponding correlation spectrum ($\theta_p + \theta_d$). Figure 2(c) shows the coplanarity spectrum for all proton angles with $\bar{\theta}_d = 10°$. The coplanarity angle is defined as $x = (x_p/\sin\theta_p) + (x_d/\sin\theta_d)$, where $x_p$ and $x_d$ are the angles relative to the horizontal plane of the proton and deuteron trajectory, respectively. Finally, Fig. 2(d) shows a typical differential-range spectrum in an experimental situation different from the one in Fig. 2(a)–(c), namely $\bar{\theta}_d = 35°$, for 316-MeV incident protons.

The relatively wide spectrum observed for the coplanarity angle is not as bad as it might seem if one realizes that through projection of the vertical scattering angles $x_p$ and $x_d$ on the plane perpendicular to the beam at the target, these angles and therefore their error are multiplied by typical factors of 4.6 on the deuteron side, 1.5 on the proton side (these numbers are valid for 12.5° deuterons and 130° protons). Furthermore, be-

TABLE IV. $pd$ differential cross section at 316 MeV.

| Proton laboratory scattering angle $\theta_{p\,\mathrm{lab}}$ (deg) | Laboratory differential cross section and error $\left(\frac{d\sigma}{d\Omega}\right)_{\mathrm{lab}} \pm \Delta\left(\frac{d\sigma}{d\Omega}\right)_{\mathrm{lab}}$ ($\mu$b/sr) | Proton center-of-mass scattering angle $\theta_{p\,\mathrm{c.m.}}$ (deg) | $\cos\theta_{p\,\mathrm{c.m.}}$ | Center-of-mass differential cross section and error $\left(\frac{d\sigma}{d\Omega}\right)_{\mathrm{c.m.}} \pm \Delta\left(\frac{d\sigma}{d\Omega}\right)_{\mathrm{c.m.}}$ ($\mu$b/sr) | Momentum transfer squared $-t$ (GeV/$c$)$^2$ |
|---|---|---|---|---|---|
| 109.0 | 40.4 ± 0.7 | 139.9 | −0.765 | 74.4 ± 1.5 | 0.939 |
| 111.0 | 39.9 ± 0.7 | 141.4 | −0.782 | 79.7 ± 1.5 | 0.946 |
| 113.5 | 38.5 ± 0.7 | 143.3 | −0.801 | 81.3 ± 1.6 | 0.958 |
| 122.3 | 34.8 ± 0.8 | 149.4 | −0.861 | 87.0 ± 1.9 | 0.990 |
| 124.7 | 38.6 ± 0.8 | 151.0 | −0.875 | 100.0 ± 2.0 | 0.997 |
| 127.1 | 40.7 ± 0.8 | 152.5 | −0.887 | 111.0 ± 2.0 | 1.004 |
| 130.2 | 38.1 ± 0.7 | 154.4 | −0.902 | 111.0 ± 2.0 | 1.01 |
| 132.6 | 38.6 ± 0.8 | 155.9 | −0.913 | 117.0 ± 2.0 | 1.02 |
| 135.0 | 37.8 ± 0.8 | 157.3 | −0.923 | 120.0 ± 3.0 | 1.02 |
| 137.4 | 34.5 ± 0.8 | 158.7 | −0.932 | 112.0 ± 3.0 | 1.03 |
| 140.1 | 38.6 ± 0.7 | 160.2 | −0.941 | 130.0 ± 2.0 | 1.03 |
| 142.7 | 41.6 ± 0.7 | 161.6 | −0.949 | 146.0 ± 3.0 | 1.04 |
| 145.95 | 39.9 ± 0.6 | 163.4 | −0.958 | 148.0 ± 2.0 | 1.04 |

cause only two vertical coordinates were available in each telescope, the rejection of spurious sparks could not be as efficient as for horizontal projections. The results obtained with checks one and two above are probably better than those for which check three has been added. The cross sections presented in the next part were obtained without coplanarity requirement (checks one and two only).

## RESULTS AND DISCUSSION

The cross sections were first calculated for every proton-angle bin as described in the previous part. A weighted average was then obtained taking two bins at a time. The results are given in Tables I to IV. The data in these tables are differential cross sections averaged over a 2.5° interval for $\theta_{\rm pcm} \leq 121°$, over 2° for $\theta_{\rm pcm}$ between 131 and 144°, over 2.4° for $\theta_{\rm pcm}$ between 148 and 159°, and 2.6° for $\theta_{\rm pcm}$ larger than 160° (the angle limits given are for 590-MeV protons, and will be slightly different at the three other energies).

Figure 3 shows $\log(d\sigma/d\Omega)_{p_{\rm c.m.}}$ as a function of $\cos(\theta_{p_{\rm c.m.}})$ at 590, 470, 364, and 316 MeV.[13] The errors in Tables I to IV and Fig. 3 are statistical only.

Possible systematic errors are as follows: (a) at a given energy, over the angular range presented, ±5%; this number includes ±3% uncertainty in the target areal density and ±4% error in $\epsilon_{sc}$; (b) from one energy to any other, ±8%; the latter number includes 5% for the $^{12}C(p, pn)^{11}C$ cross-section uncertainty, 1.5% for statistics in the monitor calibration, and 5% for uncertainties on beam characteristics reproducibility (beam-spot size, position at the monitor target, and divergence). The precision of angle measurements is estimated as (a) ±0.1° on the reproducibility of $\theta_p$, (b) ±0.01° on the reproducibility of $\theta_d$, and (c) ±0.025° for the absolute position of the deuteron counter relative to the beam line (0.3 cm at 600 cm).

A comparison of the data at the different energies, as plotted in Fig. 3, shows that the backward peaking is present at all four energies, and that the cross section is very nearly linearized in the $\cos\theta_{p_{\rm c.m.}}$ semilogarithmic representation for $\cos\theta_{p_{\rm c.m.}} \leq -0.6$. As $\cos\theta_{p_{\rm c.m.}} = 1 + (t/2p_{\rm c.m.}^2)$, where $-t$ is the four-momentum transfer, it appears that the cross section in the region of the backward peak can be represented by the function

$$d\sigma'/d\Omega = A\exp(-at),$$

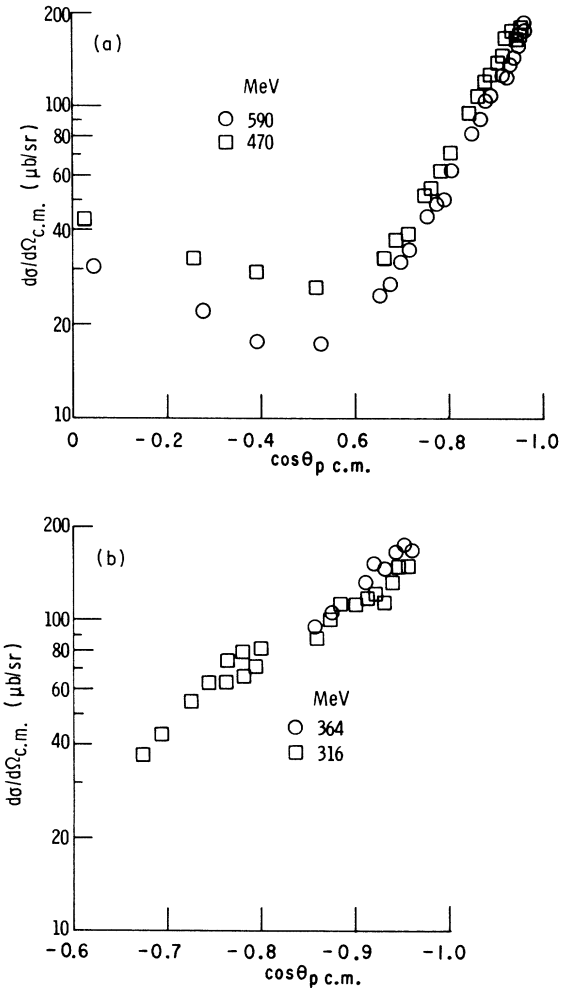


FIG. 3. Cross-section data obtained in this experiment, plotted as a function of $\cos\theta_{p\ \rm c.m.}$; $\theta_{p\ \rm c.m.}$ being the c.m. proton scattering angle. (a) shows the data at 590 and 470 MeV, for laboratory proton angles between 60 and 145°. (b) shows the 364- and 316-MeV data, for laboratory angles between 100 and 146°.

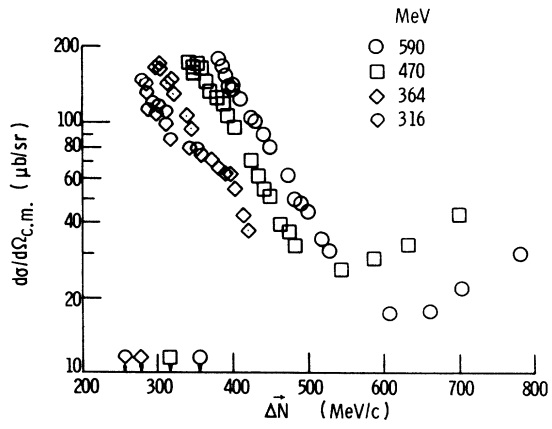


FIG. 4. The results of this experiment plotted as a function of $|\vec{\Delta}_n| = |\vec{d}_{\rm out}/2 - \vec{p}_{\rm in}|$, the Fermi momentum of the nucleon exchanged. The arrows indicate minimum values of $\vec{\Delta}_n$ at the different energies, occurring at 180° scattering angle.

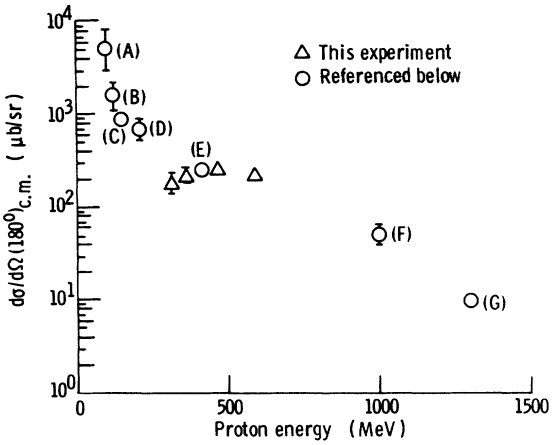


FIG. 5. The 180° c.m. cross section obtained by extrapolating the data in Fig. 3, plotted as a function of the proton incident laboratory energy. Data point (A) through (G) are from other experiments. (A) in Ref. 15, (B) in Ref. 16, (C) in Ref. 14, (D) in Ref. 17, (E) in Ref. 9, (F) in Ref. 2, and (G) in Ref. 1.

where $a$ has the values $6.85 \pm 0.1$, $7.53 \pm 0.2$, $8.55 \pm 0.2$, and $6.7 \pm 2.0$ [in $(\mathrm{GeV}/c)^{-2}$] at 590, 470, 364, and 316 MeV, respectively. However, if in the region of the backward peak the reaction mechanism is dominantly of an exchange nature, the cross section would have to be related to the Fermi momentum of the particle exchanged. In a single-nucleon exchange process, the Fermi momentum of the nucleon exchanged is given by (see also Ref. 4)

$$\vec{\Delta}_n = \frac{\vec{d}_{\mathrm{out}}}{2} - \vec{p}_{\mathrm{in}}$$

where $\vec{d}_{\mathrm{out}}$ and $\vec{p}_{\mathrm{in}}$ are the center-of-mass momenta of the outgoing deuteron and incoming proton, respectively. The magnitude of $\vec{\Delta}$ is then related to the scattering angle $\theta_{p_{\mathrm{c.m.}}}$ by

$$|\vec{\Delta}_n| = p_{\mathrm{c.m.}} \sqrt{\cos\theta_{p_{\mathrm{c.m.}}} + \tfrac{5}{4}}\,.$$

As can be seen in Fig. 4, a representation of all data as a function of $|\vec{\Delta}_n|$ does not align the points taken at different energies on a single smooth curve, although it tends to put them much closer together than a $-t$ representation would.

By extrapolating visually to $\cos\theta_{p_{\mathrm{c.m.}}} = -1.0$ straight line fits in Fig. 3 we find values of $(d\sigma'/d\Omega)_{\mathrm{c.m.}}$ at 180° shown in Fig. 5. Data from other experiments have been included (see references in caption of Fig. 5). The results of Refs. 9 and 10 have been left out. The energy region between 100 and 300 MeV shows a fast drop of the c.m. cross section with increasing energy and is well understood (Ref. 8) in terms of single-neutron exchange and multiple scattering; the cross section is directly related to $|\varphi(\Delta)|^2$, the momentum-space single-particle deuteron wave function squared. Around 300 MeV a definite flattening of the 180° cross section is observed. It appears likely that the cross section starts to decrease rapidly again just above 600 MeV. Figure 5 gives a striking demonstration of the presence of another mechanism at work beside single-nucleon exchange and multiple scattering, or possibly of the existence of another component in the deuteron ground-state wave function beside the known $s$ and $d$ states.

---

*Present address: DESY, Notkestieg 1, 2000 Hamburg-58, Germany.

†Work supported by the Swiss Institute for Nuclear Research (S.I.N.).

‡College of William and Mary, Williamsburg, Virginia.

§Nuclear Research Center, University of Alberta, Edmonton, Alberta, Canada.

¶Work supported in part by the Atomic Energy Control Board of Canada.

‖Miami University, Oxford, Ohio.

[1]E. Coleman, R. M. Heinz, O. E. Overseth, and D. E. Pellet, Phys. Rev. 164, 1655 (1967).

[2]G. W. Bennett, J. L. Friedes, H. Palevsky, R. J. Sutter, G. J. Igo, W. D. Simpson, G. C. Phillips, R. L. Stearns, and D. M. Corley, Phys. Rev. Letters 19, 387 (1967).

[3]J. S. Vincent, W. K. Roberts, E. T. Boschitz, L. S. Kisslinger, K. Gotow, P. C. Gugelot, C. F. Perfrisat, L. W. Swenson, and J. R. Priest, Phys. Rev. Letters 24, 236 (1970).

[4]A. K. Kerman and L. S. Kisslinger, Phys. Rev. 180, 1483 (1969).

[5]H. Arenhövel, M. Danos, and H. T. Williams, Nucl. Phys. A162, 12 (1971).

[6]N. S. Craigie and C. Wilkin, Nucl. Phys. B14, 477 (1969).

[7]C. Wilkin, private communication.

[8]E. A. Remler and R. A. Miller, private communication.

[9]O. Chamberlain and D. D. Clark, Phys. Rev. 102, 473 (1956).

[10]G. A. Leksin, Zh. Eksperim. i Teor. Fiz. 32, 440 (1957) [transl.: Soviet Phys. — JETP 5, 371 (1957)].

[11]N. E. Booth, C. Dolnick, R. J. Esterling, J. Parry, J. Scheid, and D. Sherden, Phys. Rev. D 4, 1261 (1971).

[12]J. B. Cumming, J. Hudis, A. M. Poskanzer, and S. Kaufman, Phys. Rev. 128, 2392 (1962).

[13]Part of the data has been presented in a National Aeronautics and Space Administration technical memorandum No. TM X-67943 and in Bull. Am. Phys. Soc. 17, 192 (1971).

[14]K. Kuroda, A. Michalowicz, and M. Poulet, Nucl.

Phys. 88, 33 (1966).
[15]O. Chamberlain and M. O. Stern, Phys. Rev. 94, 666 (1954).
[16]H. Postma and R. Wilson, Phys. Rev. 121, 1229 (1961).
[17]R. E. Adelberger, Ph.D. thesis, University of Rochester, 1967 (unpublished).

PHYSICAL REVIEW C VOLUME 6, NUMBER 6 DECEMBER 1972

# Half-Lives of $^{17}$N and $^{17}$F†

D. E. Alburger
*Brookhaven National Laboratory, Upton, New York 11973*

and

D. H. Wilkinson
*Brookhaven National Laboratory, Upton, New York 11973, and Oxford University, Oxford, England*

(Received 9 August 1972)

The radioactivities $^{17}$N and $^{17}$F have been produced in the reactions $^{15}$N$(t,p)^{17}$N and $^{16}$O$(d,n)$-$^{17}$F, respectively, and their half-lives have been measured by observing the decay of neutrons from $^{17}$N and 0.51-MeV $\gamma$ rays from $^{17}$F. The half-life obtained for $^{17}$N is $4.169 \pm 0.008$ sec in agreement with earlier measurements. Our value for $^{17}$F, $T_{1/2} = 64.50 \pm 0.25$ sec, is considerably lower than previous measurements. The relevance of the $^{17}$N result to the question of mirror symmetry in the $\beta$ decay of the $A = 17$ system is discussed.

## I. INTRODUCTION

The apparent violation of mirror symmetry in Gamow-Teller $\beta$ decay[1] has been searchingly reexamined during the past two years. It now appears[2] that the even-$A$ systems, in which the final body is common to the two sides of the mirror, do not, after correction for "trivial" effects associated with binding energy differences and so on, show significant evidence of a "fundamental" asymmetry. On the other hand, the odd-$A$ systems $A = 9$, 13, 17, and 25, for which data are available, still show large asymmetries that are not explained by binding energy effects in the initial states; the influence of such effects in the mirror final states has not been fully examined as yet.

The system $A = 17$ appeared[1] to show a large asymmetry $[(ft)^+/(ft)^- \approx 1.15]$; it has recently been reexamined in detail[3] from the positron-emitting side, i.e., the decay of $^{17}$Ne. The great bulk ($\approx$99%) of the $^{17}$Ne decay goes to proton-unstable states of $^{17}$F whose relative population in that decay can therefore be determined with high accuracy. This enables an accurate prediction to be made, assuming mirror symmetry, of the lifetime of $^{17}$N. The object of our present work was to remeasure the $^{17}$N lifetime in order to determine the asymmetry, if any, with accuracy.

The half-life of $^{17}$N has been measured several times previously and the mean of the reported values is $4.16 \pm 0.01$ sec.[4] However, only one half-life measurement on $^{17}$N has been reported since 1965. It was thought worthwhile to make another check on its value in view of the numerous discrepancies that have appeared in the literature during the past few years on the half-lives of various short-lived radioactivities.[5]

We have also taken the opportunity of remeasuring the half-life of $^{17}$F to complete the data on the $A = 17$ system. The mean of six previous measurements on the $^{17}$F half-life is $66.0 \pm 0.2$ sec,[4] but there has been a more recent value of $65.2 \pm 0.2$ sec, obtained by Wohlleben and Schuster,[6] that differs from the previous mean value by 5 standard deviations.

## II. EXPERIMANTAL PROCEDURES AND RESULTS

### A. $^{17}$N Half-Life

$^{17}$N was produced in the reaction $^{15}$N$(t,p)^{17}$N by bombarding targets enriched in $^{15}$N with a beam of 3.2-MeV tritons from the 3.5-MV Van de Graaff accelerator. The target was located at the center of a 1-in.-diam thin-walled glass target tube, and the detector was placed close to the target chamber. After shutting off the beam the decay of pulses from the detector was measured in a time channel analyzer as described previously.[5]

In the initial work the decay of $\beta$ rays was measured using the same target and $\beta$-ray detector